

On page 31, please delete the two paragraphs beginning on line 22, and substitute therefor:

B¹ FIGS. 51-56 depict several embodiments of heat sources in a relatively low permeability formation;

FIGS. 57-70 depict several embodiments of a heat source and production well pattern;

On page 34, please delete the paragraph beginning on line 29, and substitute therefor:

B² FIG. 133 depicts cumulative condensable hydrocarbons as a function of temperature produced by heating a coal cube;

On page 35, please delete the three paragraphs beginning on line 15 (as amended in the Preliminary Amendment), and substitute therefor:

B³ FIG. 144 depicts percentage ethene to ethane produced from a coal formation as a function of heating rate in a laboratory test;

FIG. 145 depicts product quality of fluids produced from a coal formation as a function of heating rate in a laboratory test;

FIG. 146 depicts weight percentages of various fluids produced from a coal formation for various heating rates in a laboratory test;

On page 71, please delete the paragraph beginning on line 26, and substitute therefor:

B⁴ FIG. 9 illustrates an embodiment of unit cell 404. Unit cell 404 includes heat sources 400 and production wells 402. Unit cell 404 may have six full heat sources 400a and six partial heat sources 400b. Full heat sources 400a may be closer to production

B4
well 402 than partial heat sources 400b. In addition, an entirety of each of the full heat sources 400a may be located within unit cell 404. Partial heat sources 400b may be partially disposed within unit cell 404. Only a portion of heat source 400b disposed within unit cell 404 may be configured to provide heat to a portion of a hydrocarbon containing formation disposed within unit cell 404. A remaining portion of heat source 400b disposed outside of unit cell 404 may be configured to provide heat to a remaining portion of the hydrocarbon containing formation outside of unit cell 404. Therefore, to determine a number of heat sources within unit cell 404 partial heat source 400b may be counted as one-half of full heat source 400a. In other unit cell embodiments, fractions other than 1/2 (e.g., 1/3) may more accurately describe the amount of heat applied to a portion from a partial heat source.

On page 107, please delete the paragraph beginning on line 11, and substitute therefor:

B5
FIG. 23a illustrates a cross-sectional view of an embodiment of a centralizer 581 disposed on conductor 580. FIG. 23b illustrates a perspective view of the embodiment shown in FIG. 23a. Centralizer 581 may be made of any suitable electrically insulating material that may substantially withstand high voltage at high temperatures. Examples of such materials may be aluminum oxide and/or Macor. Discs 581d may maintain positions of centralizer 581 relative to conductor 580. Discs 581d may be metal discs welded to conductor 580. Discs 581d may be tack-welded to conductor 580. Centralizer 581 may substantially electrically insulate conductor 580 from conduit 582.

On page 119, please delete the paragraph beginning on line 26, and substitute therefor:

B6
Oxidizing fluid 623 may mix with fuel fluid 621 in the oxidation region of inner conduit 638. Either oxidizing fluid 623 or fuel fluid 621, or a combination of both, may be preheated external to the combustor to a temperature sufficient to support oxidation of

B6
fuel fluid 621. Oxidation of fuel fluid 621 may provide heat generation within outer conduit 636. The generated heat may provide heat to at least a portion of a hydrocarbon containing formation proximate to the oxidation region of inner conduit 638. Products 625 from oxidation of fuel fluid 621 may be removed through outer conduit 636 outside inner conduit 638. Heat exchange between the downgoing oxidizing fluid and the upgoing combustion products in the overburden results in enhanced thermal efficiency. A flow of removed combustion products 625 may be balanced with a flow of fuel fluid 621 and oxidizing fluid 623 to maintain a temperature above autoignition temperature but below a temperature sufficient to produce substantial oxides of nitrogen. Also, a constant flow of fluids may provide a substantially uniform temperature distribution within the oxidation region of inner conduit 638. Outer conduit 636 may be, for example, a stainless steel tube. In this manner, heating of at least the portion of the hydrocarbon containing formation may be substantially uniform. As described above, the lower operating temperature may also provide a less expensive metallurgical cost associated with the heating system.

On pages 135-137, please delete Tables 2a-2g, and substitute therefor:

TABLE 2a

B7

API Gravity	A	B
20 degrees	-59906.9	83.46594
25 degrees	-43778.5	66.85148
30 degrees	-30864.5	50.67593
35 degrees	-21718.5	37.82131
40 degrees	-16894.7	31.16965
45 degrees	-16946.8	33.60297

TABLE 2b

Ethene/Ethane Ratio	<i>A</i>	<i>B</i>
0.20	-57379	83.145
0.10	-16056	27.652
0.05	-11736	21.986
0.01	-5492.8	14.234

TABLE 2c

Weight Percent of Hydrocarbons Having a Carbon Number Greater Than 25	<i>A</i>	<i>B</i>
25 %	-14206	25.123
20 %	-15972	28.442
15 %	-17912	31.804
10 %	-19929	35.349
5 %	-21956	38.849
1 %	-24146	43.394

TABLE 2d

Atomic H/C Ratio	<i>A</i>	<i>B</i>
1.7	-38360	60.531
1.8	-12635	23.989
1.9	-7953.1	17.889
2.0	-6613.1	16.364

TABLE 2e

Liquid Production (gal/ton)	<i>A</i>	<i>B</i>
14 gal/ton	-10179	21.780
16 gal/ton	-13285	25.866
18 gal/ton	-18364	32.882
20 gal/ton	-19689	34.282

TABLE 2f

Equivalent Liquid Production (gal/ton)	<i>A</i>	<i>B</i>
20 gal/ton	-19721	38.338
25 gal/ton	-23350	42.052
30 gal/ton	-39768.9	57.68

TABLE 2g

% Fischer Assay	<i>A</i>	<i>B</i>
60 %	-11118	23.156
70 %	-13726	26.635
80 %	-20543	36.191
90 %	-28554	47.084

On page 172, please delete the paragraph beginning on line 25, and substitute therefor:

FIG. 40 depicts an embodiment of in situ synthesis gas production integrated with a catalytic methanation process. For example, synthesis gas 1140 exiting production well 1142 may be supplied to catalytic methanation plant 1144. In some embodiments, it may be desirable for the composition of produced synthesis gas, which may be used as a feed

B⁸
gas for a catalytic methanation process, to have a H₂ to carbon monoxide ratio of about three to one. Methane 1146 may be produced by catalytic methanation plant 1144. Steam 1148 produced by plant 1144 may be supplied to injection well 1141 for production of synthesis gas. Examples of a catalytic methanation process are illustrated in U.S. Patent Nos. 3,922,148 to Child; 4,130,575 to Jorn et al.; and 4,133,825 to Stroud et al., which are incorporated by reference as if fully set forth herein.

On page 202, please delete the paragraph beginning on line 4, and substitute therefor:

B⁹
Alternatively, square patterns may be provided with production wells placed, for example, in the center of each third square, resulting in nine heat sources for each production well. Production wells may be placed within each fifth square in a square pattern, which may result in twenty-five heat sources for each production well.

On page 203, please delete the two paragraphs beginning on line 15, and substitute therefor:

B¹⁰
FIG. 67 illustrates a pattern of production wells 2760 with inner triangular ring 2766 and outer hexagonal ring 2768. In this pattern, production wells 2760 may be spaced at a distance of 2s. Heat sources 2762 may be located at apices of inner ring 2766 and outer ring 2768. Inner triangular ring 2766 may contribute three equivalent heat sources per production well 2760. Outer hexagonal ring 2768 containing three heater wells may contribute one equivalent heat source per production well 2760. Thus, a total of four equivalent heat sources may provide heat to production well 2760.

FIG. 68 illustrates a pattern of production wells with one inner triangular ring of heat sources surrounding each production well and one irregular hexagonal outer ring. Production wells 2760 may be surrounded by ring 2770 of three heat sources 2762. Production wells 2760 may be spaced at a distance of 3s. Irregular hexagonally shaped

B10 ring 2772 of nine heat sources 2762 may surround ring 2770. This pattern may result in a ratio of heat sources 2762 to production wells 2760 of nine.

On page 206, please delete the paragraph beginning on line 12, and substitute therefor:

B11 Power generation unit 2822 may be configured for extracting useable energy from the first portion of stream 2818. For example, stream 2818 may be produced under pressure. In this manner, power generation unit 2822 may include a turbine configured to generate electricity from the first portion of stream 2818. The power generation unit may also include, for example, a molten carbonate fuel cell, a solid oxide fuel cell, or other type of fuel cell. The facilities may be further configured such that the extracted useable energy may be provided to user 2824. User 2824 may include, for example, surface facilities 2800, a heat source disposed within a formation, and/or a consumer of useable energy.

On page 212, please delete the paragraph beginning on line 10, and substitute therefor:

B12 FIG. 75 illustrates an example of another pattern of heat sources 3000 and production wells 3002. Midlines 3006 are formed equidistant from the two production wells 3002, and perpendicular to a line connecting such production wells. Unit cell 3014 is determined by intersection of midlines 3006 at vertices 3008. Twelve heat sources 3000 are counted in unit cell 3014 by a method as described in the above embodiments, of which six are whole sources of heat, and six are one third sources of heat (with the other two thirds of heat from such six wells going to other patterns). Thus, a ratio of heat sources 3000 to production wells 3002 is determined as 8:1 for the pattern illustrated in FIG. 75. An example of a pattern of heat sources is illustrated in U.S. Patent No. 2,923,535 issued to Ljungstrom, which is incorporated by reference as if fully set forth herein.

On page 216, please delete the paragraph beginning on line 4, and substitute therefor:

B13

FIG. 81b illustrates a comparison plot between the average pattern temperature and temperatures at the coldest spots for each pattern, as a function of time when heaters are turned off after the average temperature reaches a target value. As shown in FIG. 81b, an average temperature 3120 of the formation reaches a target temperature (about 340 °C) in approximately 3 years. As shown in FIG. 81b, a temperature at the coldest point within the triangular pattern 3118 reaches the target temperature (about 340 °C) about 0.8 years later. In this manner, a total process time for such a triangular pattern is about 3.8 years when the heat input is discontinued when the target average temperature is reached. As shown in FIG. 81b, a temperature at the coldest point within the triangular pattern reaches the target temperature (about 340 °C) before a temperature at the coldest point within the square pattern 3117 or a temperature at the coldest point within the hexagonal pattern 3114 reaches the target temperature. A temperature at the coldest point within the hexagonal pattern, however, reaches the target temperature after an additional time of about 2 years when the heaters are turned off upon reaching the target average temperature. Therefore, a total process time for a hexagonal pattern is about 5.0 years. In this manner, a total process time for heating a portion of a formation with a triangular pattern is 1.2 years less (approximately 25 %) than a total process time for heating a portion of a formation with a hexagonal pattern. In a preferred mode, the power to the heaters may be reduced or turned off when the average temperature of the pattern reaches a target level. This prevents overheating the resource, which wastes energy and produces lower product quality. The triangular pattern has the most uniform temperatures and the least overheating. Although a capital cost of such a triangular pattern may be approximately the same as a capital cost of the hexagonal pattern, the triangular pattern may accelerate oil production and requires a shorter total process time. In this manner, such a triangular pattern may be more economical than a hexagonal pattern.

On page 225, please delete the paragraph beginning on line 14, and substitute therefor:

B14 In FIG. 90, a plot of gauge pressure versus temperature is depicted (in FIGS. 90-96 the pressure is indicated in bars). Lines representing the fraction of products with carbon numbers greater than about 25 were plotted. For example, when operating at a temperature of 375 °C and a pressure of 4.5 bars absolute, 15 % of the produced fluid hydrocarbons had a carbon number equal to or greater than 25. At low pyrolysis temperatures and high pressures, the fraction of produced fluids with carbon numbers greater than about 25 decreases. Therefore, operating at a high pressure and a pyrolysis temperature at the lower end of the pyrolysis temperature zone tends to decrease the fraction of fluids with carbon numbers greater than 25 produced from oil shale.

On page 225, please delete the paragraph beginning on line 24 (as amended in the Preliminary Amendment), and substitute therefor:

B15 FIG. 91 illustrates oil quality produced from an oil shale formation as a function of pressure and temperature. Lines indicating different oil qualities, as defined by API gravity, are plotted. For example, the quality of the produced oil was 40° API when pressure was maintained at about 11.1 bars absolute and a temperature was about 375 °C. As described in above embodiments, low pyrolysis temperatures and relatively high pressures may produce a high API gravity oil.

On page 226, please delete the two paragraphs beginning on line 1 (as amended in the Preliminary Amendment), and substitute therefor:

B16 FIG. 92 illustrates an ethene to ethane ratio produced from an oil shale formation as a function of pressure and temperature. For example, at a pressure of 21.7 bars absolute and a temperature of 375 °C, the ratio of ethene to ethane is approximately 0.01. The volume ratio of ethene to ethane may predict an olefin to alkane ratio of

B14 hydrocarbons produced during pyrolysis. To control olefin content, operating at lower pyrolysis temperatures and a higher pressure may be beneficial. Olefin content in above described embodiments may be reduced by operating at low pyrolysis temperature and a high pressure.

FIG. 93 depicts the dependence of yield of equivalent liquids produced from an oil shale formation as a function of temperature and pressure. Line 3340 represents the pressure-temperature combination at which $8.38 \times 10^{-5} \text{ m}^3$ of fluid per kilogram of oil shale (20 gallons/ton). The pressure/temperature plot results in a line 3342 for the production of total fluids per ton of oil shale equal to $1.05 \times 10^{-4} \text{ m}^3/\text{kg}$ (25 gallons/ton). Line 3344 illustrates that $1.21 \times 10^{-4} \text{ m}^3$ of fluid is produced from 1 kilogram of oil shale (30 gallons/ton). For example, at a temperature of about 325 °C and a pressure of about 14.8 bars absolute the resulting equivalent liquids was $8.38 \times 10^{-5} \text{ m}^3/\text{kg}$. As temperature of the retort increased and the pressure decreased the yield of the equivalent liquids produced increased. Equivalent liquids produced was defined as the amount of liquid equivalent to the energy value of the produced gas and liquids.

On page 227, please delete the paragraph beginning on line 19 (as amended in the Preliminary Amendment), and substitute therefor:

B17 FIG. 97 illustrates the effect of pressure and temperature within an oil shale formation on a ratio of olefins to paraffins. The relationship of the value of one of the properties (R) with temperature has the same functional form as the pressure-temperature relationships previously discussed. In this case the property (R) can be explicitly expressed as a function of pressure and temperature.

$$R = \exp[F(P)/T] + G(P)$$

$$F(P) = f_1 * (P)^3 + f_2 * (P)^2 + f_3 * (P) + f_4$$

$$G(P) = g_1 * (P)^3 + g_2 * (P)^2 + g_3 * (P) + g_4$$

B17 wherein R is a value of the property, T is the absolute temperature (in Kelvin), $F(P)$ and $G(P)$ are functions of pressure representing the slope and intercept of a plot of R versus $1/T$.

On page 228, please delete the paragraph beginning on line 6, and substitute therefor:

B18 FIG. 97 is an example of such a plot for olefin to paraffin ratio. Data from the above experiments were compared to data from other sources. Isobars were plotted on a temperature versus olefin to paraffin ratio graph using data from a variety of sources. Data from the above described experiments included an isobar at 1 bar absolute 3360, 2.5 bars absolute 3362, 4.5 bars absolute 3364, 7.9 bars absolute 3366, and 14.8 bars absolute 3368. Additional data plotted included data from a surface retort, data from Ljungstrom 3361, and data from ex situ oil shale studies conducted by Lawrence Livermore Laboratories 3363. As illustrated in FIG. 97, the olefin to paraffin ratio appears to increase as the pyrolysis temperature increases. However, for a fixed temperature, the ratio decreases rapidly with an increase in pressure. Higher pressures and lower temperatures appear to favor the lowest olefin to paraffin ratios. At a temperature of about 350 °C and a pressure of about 7.9 bars absolute 3366, a ratio of olefins to paraffins was approximately 0.01. Pyrolyzing at reduced temperature and increased pressure may decrease an olefin to paraffin ratio. Pyrolyzing hydrocarbons for a longer period of time, which may be accomplished by increasing pressure within the system, tends to result in a lower average molecular weight oil. In addition, production of gas may increase and a non-volatile coke may be formed.

On page 238, please delete the paragraph beginning on line 9, and substitute therefor:

B19 As shown in Table 4, gas produced according to an embodiment described herein may be treated and sold through existing natural gas systems. In contrast, gas produced

B19
by typical in situ gasification processes may not be treated and sold through existing natural gas systems. For example, a heating value of the gas produced by gasification with air was 6000 KJ/m³, and a heating value of gas produced by gasification with oxygen was 11,439 KJ/m³. In contrast, a heating value of the gas produced by thermal conductive heating was 39,159 KJ/m³.

On page 244, please delete the paragraph beginning on line 10 (as amended in the Preliminary Amendment), and substitute therefor:

B20
Hydrocarbon fluids were produced from a portion of a coal formation by an in situ experiment conducted in a portion of a coal formation. The coal was high volatile bituminous C coal. It was heated with electrical heaters. FIG. 136 illustrates a cross-sectional view of the in situ experimental field test system. As shown in FIG. 136, the experimental field test system included coal formation 3802 within the ground and grout wall 3800. Coal formation 3802 dipped at an angle of approximately 36° with a thickness of approximately 4.9 meters. FIG. 137 illustrates a location of heat sources 3804a, 3804b, 3804c, production wells 3806a, 3806b, and temperature observation wells 3808a, 3808b, 3808c, 3808d used for the experimental field test system. The three heat sources were disposed in a triangular configuration. Production well 3806a was located proximate a center of the heat source pattern and equidistant from each of the heat sources. A second production well 3806b was located outside the heat source pattern and spaced equidistant from the two closest heat sources. Grout wall 3800 was formed around the heat source pattern and the production wells. The grout wall was formed of 24 pillars. Grout wall 3800 was configured to inhibit an influx of water into the portion during the in situ experiment. In addition, grout wall 3800 was configured to substantially inhibit loss of generated hydrocarbon fluids to an unheated portion of the formation.

On page 250, please delete the paragraph beginning on line 2 (as amended in the Preliminary Amendment), and substitute therefor:

B24

An experiment was conducted on the coal formation treated according to the in situ conversion process to measure the uniform permeability of the formation after pyrolysis. After heating a portion of the coal formation, a ten minute pulse of CO₂ was injected into the formation at first production well 3806a and produced at well 3804a, as shown in FIG. 137. The CO₂ tracer test was repeated from production well 3806a to well 3804b and from production well 3806a to well 3804c. As described above, each of the three different heat sources were located equidistant from the production well. The CO₂ was injected at a rate of 4.08 m³/h (144 standard cubic feet per hour). As illustrated in FIG. 147, the CO₂ reached each of the three different heat sources at approximately the same time. Line 3900 illustrates production of CO₂ at heat source 3804a, line 3902 illustrates production of CO₂ at heat source 3804b, and line 3904 illustrates production of CO₂ at heat source 3804c. As shown in FIG. 149, yield of CO₂ 3910 from each of the three different wells was also approximately equal over time. Such approximately equivalent transfer of a tracer pulse of CO₂ through the formation and yield of CO₂ from the formation indicated that the formation was substantially uniformly permeable. The fact that the first CO₂ arrival only occurs approximately 18 minutes after start of the CO₂ pulse indicates that no preferential paths had been created between well 3806a and wells 3804a, 3804b, and 3804c.

On page 251, please delete the paragraph beginning on line 25, and substitute therefor:

B22

From FIG. 151, the maximum natural water inflow is approximately 5 kg/h as indicated by arrow 3920. Arrows 3922, 3924, and 3926 represent injected water rates of about 2.7 kg/h, 5.4 kg/h, and 11 kg/h, respectively, into central well 3806a of FIG. 137. Production of synthesis gas is at heater wells 3804a, 3804b, and 3804c. FIG. 151 shows that the synthesis gas production per unit volume of water injected decreases at arrow 3922 at approximately 2.7 kg/h of injected water or 7.7 kg/h of total water inflow. The reason for the decrease is that steam is flowing too fast through the coal seam to allow the

B22
reactions to approach equilibrium conditions.

On page 254, please delete the paragraph beginning on line 17, and substitute therefor:

B23
Table 6 includes a composition of synthesis gas produced during a run of the in situ coal field experiment.

On page 256, please delete the paragraph beginning on line 4 (as amended in the Preliminary Amendment), and substitute therefor:

B24
FIG. 160 is a plot of calculated equilibrium wet mole fractions for a coal reaction with water. Equilibrium wet mole fractions are shown for water 4006, H₂ 4008, carbon monoxide 4010, and carbon dioxide 4012 as a function of temperature at a pressure of 2 bars absolute. At 390 °C, the produced gas includes about 89 % water, about 7 % H₂, and about 4 % carbon dioxide. At 500 °C, the produced gas includes about 66 % water, about 22 % H₂, about 11 % carbon dioxide, and about 1 % carbon monoxide. At 700 °C, the produced gas includes about 18 % water, about 47.5 % H₂, about 12 % carbon dioxide, and about 22.5 % carbon monoxide.

On page 257, please delete the paragraph beginning on line 11 (as amended in the Preliminary Amendment), and substitute therefor:

B25
In the embodiments of FIG. 161, the methane reactions in Equations (4) and (5) are included. The calculations set forth herein assume that char is only made of carbon and that there is an excess of carbon to steam. About 890 MW of energy 4024 is required to pyrolyze about 105,800 metric tons per day of coal. The pyrolysis products 4028 include liquids and gases with a production of 23,000 cubic meters per day. The pyrolysis process also produces about 7,160 metric tons per day of water 4030. In the synthesis gas stage about 57,800 metric tons per day of char with injection of 23,000

B²⁵ metric tons per day of steam 4032 and 2,000 MW of energy 4034 with a 20% conversion will produce 12,700 cubic meters equivalent oil per day of synthesis gas 4038.

On page 263, please delete the paragraph beginning on line 2, and substitute therefor:

B²⁶ FIG. 177 illustrates the pressure at the wellhead of the injection wells as a function of time during the simulation. The pressure decreased from about 114 bars absolute to about 19 bars absolute over the first 370 days. The decrease in the pressure was due to removal of water from the coal formation. Pressure then started to increase substantially as carbon dioxide injection started at 370 days. The pressure reached a maximum of about 98 bars absolute. The pressure then began to gradually decrease after 480 days. At about 1440 days, the pressure increased again to about 98 bars absolute due to the increase in the carbon dioxide injection rate. The pressure gradually increased until about 3640 days. The pressure jumped at about 3640 days because the production well was closed off.

On page 271, please delete the paragraph beginning on line 11 (as amended in the Preliminary Amendment), and substitute therefor:

B²⁷ A three-dimensional (3-D) simulation model was used to simulate an in situ conversion process for a tar sand formation. A heat injection rate was calculated using a separate numerical code (CFX; AEA Technology, Oxfordshire, UK). The heat injection rate was calculated at 500 watts per foot (1640 watts per meter). The 3-D simulation was based on a dilation-recompaction model for tar sands. A target zone thickness of 50 meters was used. Input data for the simulation were based on average reservoir properties of the Grosmont formation in northern Alberta, Canada as follows:

Depth of target zone = 280 meters;
Thickness = 50 meters;

027
Porosity = 0.27;
Oil saturation = 0.84;
Water saturation = 0.16;
Permeability = 1000 millidarcy;
Vertical permeability versus horizontal permeability = 0.1;
Overburden = shale; and
Base rock = wet carbonate.

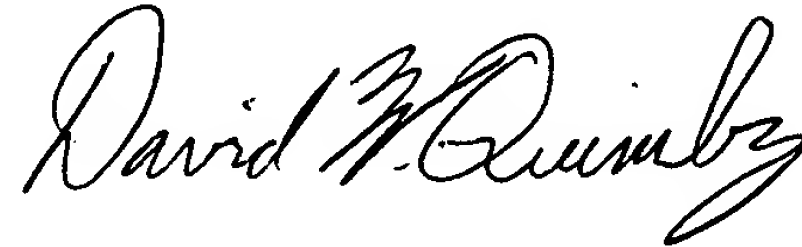
Six component fluids were used based on fluids found in Athabasca tar sands. The six component fluids were: heavy fluid; light fluid; gas; water; pre-char; and char. The spacing between wells was set at 9.1 meters on a triangular pattern. Eleven horizontal heaters with a 300 m heater length were used with heat outputs set at the previously calculated value of 1640 watts per meter.

On page 272, please delete the paragraph beginning on line 7, and substitute therefor:

028
FIG. 171 illustrates a plot of a ratio of heat content of produced fluids from a reservoir against heat input to heat the reservoir versus time (in days). Plot 4752 illustrates the ratio versus time for heating an entire reservoir to a pyrolysis temperature. Plot 4750 illustrates the ratio versus time for allowing partial drainage in the reservoir into a selected pyrolyzation section. FIG. 171 demonstrates that allowing partial drainage in the reservoir tends to increase the heat content of produced fluids versus heating the entire reservoir, for a given heat input into the reservoir.

It is believed that no fees are due in association with the filing of this document.
If any fees are required, please appropriately charge those fees to Conley, Rose & Tayon,
P.C. Deposit Account Number 50-1505/5659-03300/EBM.

Respectfully submitted,



David W. Quimby
Reg. No. 39,338

Attorney for Applicant

CONLEY, ROSE & TAYON, P.C.
P.O. BOX 398
AUSTIN, TX 78767-0398
(512) 476-1400 (voice)
(512) 703-1250 (facsimile)

Date: Feb. 13, 2002